

Spontaneous rotating vortex lattices in a pumped decaying condensate

Jonathan Keeling¹ and Natalia G. Berloff²

¹*Cavendish Laboratory, University of Cambridge, J.J.Thomson Ave., Cambridge CB3 0HE, UK*

²*Department of Applied Mathematics and Theoretical Physics,
University of Cambridge, Cambridge, CB3 0WA, UK*

Injection and decay of particles in an inhomogeneous quantum condensate can significantly change its behaviour. We model trapped, pumped, decaying condensates by a complex Gross-Pitaevskii equation and analyse the density and currents in the steady state. With homogeneous pumping, rotationally symmetric solutions are unstable. Stability may be restored by a finite pumping spot. However if the pumping spot is larger than the Thomas-Fermi cloud radius, then rotationally symmetric solutions are replaced by solutions with spontaneous arrays of vortices. These vortex arrays arise without any rotation of the trap, spontaneously breaking rotational symmetry.

PACS numbers: 03.75.Kk, 47.37.+q, 71.36.+c, 71.35.Lk

While much of the possible physics of quantum condensates has been examined in experiments on atomic gases, superfluid Helium and superconductors, there has recently been much interest in examples of condensates of quasiparticle excitations, such as excitons [1, 2] (bound electron-hole pairs), exciton-polaritons [3, 4, 5] (superpositions of quantum well excitons and microcavity photons), and magnons (spin-wave excitations) both in magnetic insulating crystals [6, 7] [33] and in superfluid ³He [8, 9, 10]. One particular difference shown by these systems is that the quasiparticles have finite lifetimes, and as a result, they can be made to form condensates out of equilibrium, which are best understood as a steady state balance between pumping and decay, rather than true thermal equilibrium. The effects of pumping and decay in these condensates have been the subject of several recent works [5, 11, 12, 13, 14, 15, 16, 17, 18, 19, 20] which have shown that even when collisions can rapidly thermalise the energy distribution of a system, there may yet be noticeable effects associated with the energy scale introduced by the pumping and decay.

The Gross-Pitaevskii equation (GPE) has been applied to successfully describe many features of equilibrium condensates when far in the condensed regime, including density profiles, the dynamics of vortices, hydrodynamic modes — see e.g. [21] and Refs. therein. Using a mean-field description of the condensate, e.g. [18, 19, 20], one can recover a complex Gross-Pitaevskii equation (cGPE), including terms representing gain, loss and an external trapping potential. This letter studies the interplay between pumping and decay and the external trapping potential in the context of the cGPE in order to illustrate some of the differences between equilibrium and non-equilibrium condensates. In the absence of trapping, this is the celebrated complex Ginzburg-Landau equation that describes a vast variety of phenomena [22] from nonlinear waves to second-order phase transitions, from superconductivity to liquid crystals and cosmic strings and binary fluids [23]. What is of interest in this letter is how pumping and decay, described in the cGPE modify

behaviour compared to the regular GPE as is widely applied to spatially inhomogeneous equilibrium quantum condensates [21]. Spatial inhomogeneity, due to either engineered and disorder potentials, has been studied for both excitons [1] and polaritons [3, 4, 5, 24].

By looking for steady state solutions to the cGPE, we find that a density-dependent gain rate combined with spatial inhomogeneity leads to steady-state currents, connecting regions of net gain with those of net loss. These supercurrents in turn affect the density profile (as is already well known in the case of solutions with vorticity), and so pumping and decay can significantly alter the density profile of a trapped condensate. The effects of steady-state current flows in the absence of pumping were considered in Refs. [25, 26]. By studying the stability of these steady state solutions, one finds that with homogeneous pumping these solutions become unstable to breaking of rotational symmetry. Stability can be restored by reducing the size of the pumping spot to be comparable to the self-consistent size of the condensate cloud (set by the balance of pumping and decay). By increasing the pump spot size (or by decreasing the pump strength), the rotationally symmetric solutions again become unstable, and are replaced by solutions with vortex lattices. The observation of vortices driven by the combination of particle flux and spatial inhomogeneity has been seen experimentally [5]; our results indicate that such vortex solutions can arise even with symmetric traps. Our findings show the existence of new phenomena in the already rich world of complex Ginzburg-Landau equations [22] that play an enormous role in our understanding of non-equilibrium physics and pattern formation [27].

Our cGPE can be derived as the gradient expansion of the saddle point equation of a non-equilibrium path-integral theory of polariton condensation [19, 20]. However, to provide insight into its meaning, we instead describe here the physical origin of the terms it contains. The form of the cGPE depends on whether one considers coherent or incoherent pumping. Coherent pumping, injecting particles directly into the condensate at an

energy ω_0 , is described by a source term $\partial_t \psi = F e^{i\omega_0 t}$ [28]. We instead consider non-resonant pumping, and thus we introduce stimulated scattering into the condensate, $\partial_t \psi|_{\text{gain}} = \gamma \psi$. A similar term $\partial_t \psi|_{\text{loss}} = -\kappa \psi$ describes particle decay, i.e. loss, and so we introduce $\gamma_{\text{eff}} = \gamma - \kappa$. With such gain and loss, the dynamics is unstable and trivial; if gain exceeds loss, the condensate grows indefinitely, if loss exceeds gain, the condensate vanishes. In practice, for non-resonantly pumped solid-state systems, the gain is saturable — it tries to bring the condensate density into chemical equilibrium with some external particle density. The simplest model of such a process is a density-dependent rate of gain, $\partial_t \rho|_{\text{gain}} = (\gamma - \Gamma \rho) \rho$, which tries to establish equilibrium at $\rho = \gamma/\Gamma$. A closely related model of saturation, considering a reservoir of non-condensed particles was studied in [17]; the steady state behaviours of both models are very similar. We combine these terms and write the complex GPE in the following form

$$i\hbar \partial_t \psi = \left[-\frac{\hbar^2 \nabla^2}{2m} + V(r) + U|\psi|^2 + i(\gamma_{\text{eff}} - \Gamma|\psi|^2) \right] \psi, \quad (1)$$

where $V(r)$ is an external trapping potential, and U is the strength of the δ -function interaction (pseudo) potential.

We will look for steady state solutions and introduce the chemical potential, μ , in the usual way, via $i\hbar \partial_t \psi(t) = \mu \psi(t)$. In this equation μ is a free parameter to be determined from the balance of gain and loss; neither the chemical potential nor total number of particles is externally imposed. We will illustrate how the interaction of spatial inhomogeneity with pumping and decay modifies the density profile by studying how the profile depends on pumping strength in a number of cases.

We consider the classic example of a parabolic trapping potential in two dimensions. For this problem, two dimensionless parameters control the behaviour. We can write the potential as $V(r) = (\hbar\omega/2)(r^2/l^2)$, where ω is the oscillator frequency and $l = \sqrt{\hbar/m\omega}$ is the oscillator length. Expressing lengths in units of l , energies in units of $\hbar\omega$, and rescaling $\psi \rightarrow \sqrt{\hbar\omega/2U}\psi$, yields:

$$\left(\frac{2\mu}{\hbar\omega} \right) \psi = \left[-\nabla^2 + r^2 + |\psi|^2 + i \left(\frac{2\gamma_{\text{eff}}}{\hbar\omega} - \frac{\Gamma}{U} |\psi|^2 \right) \right] \psi. \quad (2)$$

For the rest of this letter, we shall write $\tilde{\mu} = 2\mu/\hbar\omega$, and introduce the two dimensionless parameters which control the density profile: $\alpha = 2\gamma_{\text{eff}}/\hbar\omega$, and $\sigma = \Gamma/U$.

Before discussing the solutions, we give illustrative values α, σ , relevant to the polariton experiments of Refs. [3, 24]. The maximum pumping strengths considered are around ten times the threshold pumping strength; this threshold occurs when pumping matches decay rate $\gamma = \kappa$. The decay rate, found from the linewidth at low power, is $\kappa \simeq 0.13\text{meV}$, and so the pump rate may be up to $\gamma_{\text{eff}} < 1.2\text{meV}$. To find α , one needs

also the characteristic trap scale. In Ref. [24], the dis-order traps are estimated to have a depth $E_0 \simeq 0.5\text{meV}$ and size $a \simeq 3\mu\text{m}$, which with a polariton mass of $m \simeq 10^{-4}m_0$ yields a trap frequency $\hbar\omega = \sqrt{E_0 \hbar^2 / m a^2} \simeq 0.2\text{meV}$; hence $0 \leq \alpha \lesssim 10$. Γ is harder to estimate without a specific microscopic model; an order-of-magnitude estimate may be found from the observed blue shift (shift of chemical potential) vs pumping power. As discussed below, for weak pumping one has $\mu \simeq (\hbar\omega/2)(3\alpha/2\sigma)$, and so $\sigma \simeq 3\gamma_{\text{eff}}/2\mu$. In Ref. [3], a pump power at twice threshold, i.e. $\gamma_{\text{eff}} \sim 0.13\text{meV}$ yields a blue shift $\mu \sim 0.5\text{meV}$, giving $\sigma \simeq 0.3$, however this estimate involves considerable uncertainty.

We first discuss the rotationally symmetric steady states of Eq. (2), using fixed point iterations combined with the secant algorithm for determining $\tilde{\mu}$ for a variety of parameters. We compare the densities of the ground state with the analytical Thomas-Fermi (TF) profiles found by neglecting density gradients and assuming that supercurrents do not affect the density distributions. Figure 1 shows the density profiles for different values of α . As α increases, two effects are clear: firstly the increased pumping rate evidently leads to an increased total density of the condensate; secondly increased pumping leads to a greater flux, and so for $\alpha = 4.4$, the density profile is not the TF profile, but is suppressed in the middle, where the supercurrent is highest. The increase in total density can be described from the balance of net gain and loss; by multiplying Eq. (2) by ψ^* and integrating over all space, the imaginary part of this equation is:

$$\int d^2r (\alpha - \sigma|\psi|^2) |\psi|^2 = 0. \quad (3)$$

When pumping is not too strong, substituting the Thomas-Fermi solution $|\psi|^2 = (\tilde{\mu} - r^2)$ for $r < \sqrt{\tilde{\mu}}$ into this equation yields $\tilde{\mu} = \mu^* \equiv 3\alpha/2\sigma$.

The suppression of density due to supercurrent means that with increasing pumping, the density profile becomes increasingly sharp as supercurrent flows become important. Such results have been strongly hinted at in several microcavity polariton experiments where sharpening of the peaks of the density profile with increasing density is seen with both disorder traps [24, 29] and engineered stress traps [4].

Let us now discuss how the changes to the density profile seen above can be understood physically. The Madelung transformation, $\psi = \sqrt{\rho} e^{i\phi}$, represents Eq. (2) as a continuity equation and Bernoulli's equation:

$$\nabla \cdot [\rho \nabla \phi] = (\alpha - \sigma\rho) \rho, \quad (4)$$

$$\tilde{\mu} = |\nabla \phi|^2 + r^2 + \rho - \frac{\nabla^2 \sqrt{\rho}}{\sqrt{\rho}}. \quad (5)$$

Regions of high density imply loss, and regions of low density gain, which lead to supercurrents $\nabla \phi$, between

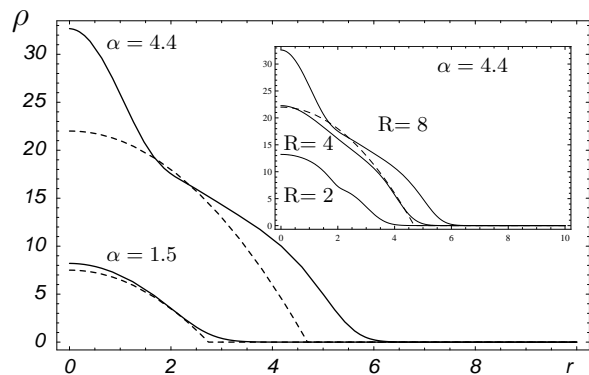


FIG. 1: The densities, $\rho(r)$, of the steady states of Eq. (2) for $\sigma = 0.3$ and $\alpha = 1.5, 4.4$ (black solid lines) as compared to the TF solutions $\rho = \mu^* - r^2, r < \sqrt{\mu^*}$ (dashed lines). The inset shows the symmetric solutions for $\alpha = 4.4$ with finite pump spot size as labelled; $R = 2, 4$ are stable, while $R = 8$ is unstable to breaking rotational symmetry.

these regions. If these supercurrents are large, they affect the Bernoulli equation, leading to a density depletion where current is largest. This is clearly seen in Fig. 1; there is net gain at large radii, and net loss at small radii, and a dip in the density profile in between these indicates a region of maximum supercurrent. The radial phase gradient associated with the current could be seen experimentally using interferograms as in e.g. [3, 5, 29]; the maximum phase difference across the cloud scales as $\Delta\phi \propto \sigma\mu^2$ and $\Delta\phi \simeq 30$, for relevant parameters.

To study stability, the time evolution of Eq. (1) is followed, using the rotationally symmetric steady-state solutions as initial conditions, and including a small perturbation. With an infinite homogeneous pump, as in Eq. (1), the solution is always unstable to angular perturbations. This instability can also be seen by considering pumping and decay as perturbative corrections to the hydrodynamic modes of a trapped 2D condensate; one finds the leading order correction to the mode energies introduces growth/decay rates which always produce growth for modes with large enough angular momentum. Physically, this instability can be understood by looking at the region just outside the condensate cloud. In this region the steady state gain is zero since it is proportional to density, however linear stability analysis for $\rho \rightarrow \rho + \delta\rho$ depends on $\partial_\rho [(\alpha - \sigma\rho)\rho] \propto \alpha - 2\sigma\rho$, which is positive outside the condensate cloud, so any small perturbation will grow. High angular momentum hydrodynamic modes of the condensate are unstable because they transfer density to the edge of the condensate.

This mechanism of instability is supported by observing that the instability is not present with a finite spot size; this ensures that outside the condensate cloud there is no gain, and so no growth. For simplicity, we treat this radial cutoff by replacing α by $\alpha(r) = \alpha\Theta(R - r)$, where Θ is the unit step function and R the cutoff radius. A

finite spot, of size comparable to the observed cloud is in fact used in current experiments [3, 4, 5]. For small R , this stabilises the radially symmetric modes. However, when R exceeds the Thomas-Fermi condensate radius, $\sqrt{\mu} \simeq \sqrt{3\alpha/2\sigma}$, the instability reappears. The subsequent time dynamics, leading to a new steady state is shown in Fig. 2. The final state is no longer stationary, but instead rotates according to: $i\hbar\partial_t\psi = (\mu - 2\Omega L_z)\psi$, where $L_z = i(x\partial_y - y\partial_x)$.

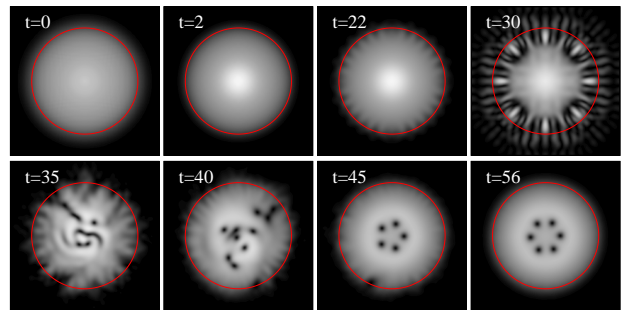


FIG. 2: (Color online) Time evolution from the rotationally symmetric steady state solution of Eq. (2) for $\sigma = 0.3, \alpha = 4.4$ when the radius of the finite pumping spot is $R = 5$ (as marked by the red line). Times are in units of $2/\omega$, where ω is frequency of harmonic trap.

As the initial problem is rotationally symmetric and non-rotating, the vortex solution spontaneously breaks rotation symmetry; either sign of vortex array is stable, but the rotationally symmetric solution is not stable. This behaviour is characteristically different from the equilibrium non-rotating trapped condensate in which vortex solutions are unstable [30], and vortices would spiral out of the condensate — with pumping and decay the dynamics shown in Fig. 2 shows that vortices spiral into the condensate. In addition, for a given radius of pump spot, more than one vortex array may be stable, the number of vortices depending on the history of the spot size; this is indicated in Fig. 3. This is similar to hysteresis effects in rotating Bose-Einstein condensates [31], but the external rotation is absent in the model considered. The origin of the instability — growth of condensate density outside the Thomas-Fermi radius — suggests that other models of the cGPE with a reservoir would show the same behaviour [18]; for the instability to be removed, one requires a reservoir concentrated near the minimum of the trap. In the context of the polariton condensate, this means the instability might be cured if the non-condensed exciton reservoir was highly mobile — in the language of laser theory, this corresponds to damping of instabilities by carrier diffusion.

This solution of the cGPE can be understood as vortices enlarging the cloud size to match the pump spot.

Adapting Eqs. (4,5) for a rotating solution [21] gives:

$$\nabla \cdot [\rho(\nabla\phi - \Omega \times \mathbf{r})] = (\alpha\Theta(R-r) - \sigma\rho)\rho, \quad (6)$$

$$\tilde{\mu} \simeq |\nabla\phi - \Omega \times \mathbf{r}|^2 + r^2(1 - \Omega^2) + \rho - \frac{\nabla^2 \sqrt{\rho}}{\sqrt{\rho}}. \quad (7)$$

The rotating vortex lattice solution adopted can be understood as follows; vortices lead to quantised rotation, and the density of vortices, $n_v \simeq \Omega/\pi$ ensures that $\nabla\phi \simeq \Omega \times \mathbf{r}$ mimicking solid body rotation. Neglecting the vortex core, the continuity equation, Eq. (6), thus requires $\rho \simeq \alpha/\sigma$. This implies that inside the vortex lattice there is no net radial current in contrast to the solutions with smaller R ; for the solutions with a single vortex (when $R < \sqrt{3\alpha/2\sigma}$), the combination of radial and rotational currents means such vortices are in fact “spiral vortices”. For this constant density solution to be valid (except near each vortex core) Eq. (7) requires $\Omega \simeq 1$ and $\tilde{\mu} = \rho \simeq \alpha/\sigma$. This solution persists till the edge of the vortex lattice, beyond which $\nabla\phi = N_v/r$, where N_v is the total number of vortices. The total number of vortices is then set by requiring the edge of the cloud to occur around $r = R$, leading to $N_v \simeq n_v \pi R^2 \simeq R^2$ for large R . When the vortex core is not negligible, the extra gain in the vortex core and quantum pressure corrections imply $\mu > \rho > \alpha/\sigma$. This is shown quantitatively in Fig. 3.

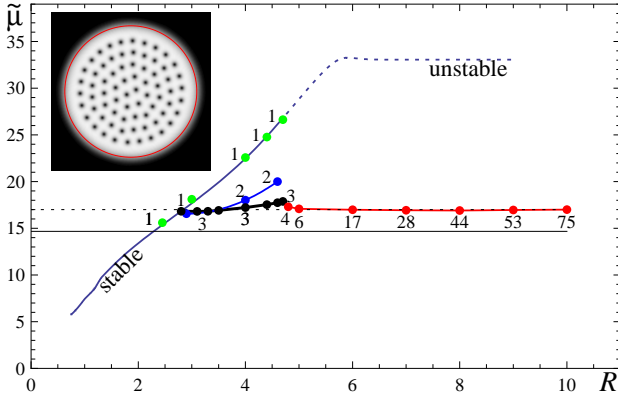


FIG. 3: (Color online) Chemical potential $\tilde{\mu}$ as a function of pumping spot size R . Numbers of vortices for the stable vortex lattice configuration are marked. Solid lines join branches of stable solutions. Dotted line corresponds to unstable radially symmetrical solutions without vortices. Horizontal solid line marks $\tilde{\mu} = \alpha/\sigma$. Inset: vortex lattice for $R = 10$.

For yet larger R , e.g. $R = 20$, no such simple rotating vortex lattice is found — for such parameters there is a residual vortex lattice in the center of the cloud, but the behaviour at the edge becomes irregular.

In conclusion, we have shown that steady-state currents connecting regions of net gain and loss can lead to significant modifications of the density profile of a quantum condensate, leading even to instability of the rotationally symmetric state and the spontaneous creation

of a vortex array. Vortices can be clearly observed as in Ref. [5] by pairs of forks in the interferogram of the emitted light. To observe the spontaneous vortex array, one would require that disorder is weak compared to the harmonic trap, which may prevent its observation in the current generation of semiconductor microcavities, however other than this hurdle, the numerical estimates place current polariton experiments in a regime in which such effects could occur.

J.K. acknowledges discussions with N. R. Cooper, I. Carusotto, P. B. Littlewood and M. H. Szymańska, and financial support from Pembroke College, Cambridge. N.G.B. acknowledges discussion with Erich Mueller and financial support from the EPSRC-UK.

-
- [1] L. V. Butov, J. Phys.: Condens. Matter **16**, R1577 (2004).
 - [2] S. Yang, A. T. Hammack, M. M. Fogler, L. V. Butov, and A. C. Gossard, Phys. Rev. Lett. **97**, 187402 (2006).
 - [3] J. Kasprzak, M. Richard, S. Kundermann, A. Baas, P. Jeambrun, J. M. J. Keeling, F. M. Marchetti, M. H. Szymanska, R. Andre, J. L. Staehli, et al., Nature **443**, 409 (2006).
 - [4] R. Balili, V. Hartwell, D. Snoke, L. Pfeiffer, and K. West, Science **316**, 1007 (2007).
 - [5] K. G. Lagoudakis, M. Wouters, M. Richard, A. Baas, I. Carusotto, R. André, L. S. Dang, and B. Deveaud-Pledran (2008), arXiv:0801.1916.
 - [6] S. O. Demokritov, V. E. Demidov, O. Dzyapko, G. A. Melkov, A. A. Serga, B. Hillebrands, and A. N. Slavin, Nature **443**, 430 (2006).
 - [7] V. E. Demidov, O. Dzyapko, S. O. Demokritov, G. A. Melkov, and A. N. Slavin, Phys. Rev. Lett. **100**, 047205 (2008).
 - [8] Y. M. Bunkov and G. E. Volovik, Phys. Rev. Lett. **98**, 265302 (2007).
 - [9] Y. M. Bunkov and G. E. Volovik, J. Low. Temp. Phys. **150**, 135 (2008).
 - [10] G. E. Volovik, cond-mat/0701180.
 - [11] F. Tassone and Y. Yamamoto, Phys. Rev. B **59**, 10830 (1999).
 - [12] G. Malpuech, A. Kavokin, A. Di Carlo, and J. J. Baumberg, Phys. Rev. B **65**, 153310 (2002).
 - [13] D. Porras, C. Ciuti, J. J. Baumberg, and C. Tejedor, Phys. Rev. B **66**, 085304 (2002).
 - [14] T. D. Doan, H. T. Cao, D. B. Tran Thoai, and H. Haug, Phys. Rev. B **72**, 085301 (2005).
 - [15] M. Wouters and I. Carusotto, Phys. Rev. B **74**, 245316 (2006).
 - [16] M. Wouters and I. Carusotto, Phys. Rev. A **76**, 043807 (2007).
 - [17] M. Wouters and I. Carusotto, Phys. Rev. Lett. **99**, 140402 (2007).
 - [18] M. Wouters, I. Carusotto, and C. Ciuti, Phys. Rev. B **77**, 115340 (2008).
 - [19] M. H. Szymańska, J. Keeling, and P. B. Littlewood, Phys. Rev. Lett. **96**, 230602 (2006).
 - [20] M. H. Szymańska, J. Keeling, and P. B. Littlewood, Phys.

- Rev. B **75**, 195331 (2007).
- [21] L. P. Pitaevskii and S. Stringari, *Bose-Einstein Condensation* (Clarendon Press, Oxford, 2003).
 - [22] I. S. Aranson and L. Kramer, Rev. Mod. Phys. **74**, 99 (2002).
 - [23] H. U. Voss, P. Kolodner, M. Abel, and J. Kurths, Phys. Rev. Lett. **83**, 3422 (1999).
 - [24] M. Richard, J. Kasprzak, R. André, R. Romestain, L. S. Dang, G. Malpuech, and A. Kavokin, Phys. Rev. B **72**, 201301(R) (2005).
 - [25] M. A. Porras, A. Parola, D. Faccio, A. Dubietis, and P. Di Trapani, Phys. Rev. Lett. **93**, 153902 (2004).
 - [26] A. Alexandrescu and V. M. Perez-Garcia, Phys. Rev. A **73**, 053610 (2006).
 - [27] M. C. Cross and P. C. Hohenberg, Rev. Mod. Phys. **65**, 851 (1993).
 - [28] M. Wouters and I. Carusotto, Phys. Rev. B **75**, 075332 (2007).
 - [29] J. Kasprzak, Ph.D. thesis, Universite Joseph Fourier, Grenoble (2006).
 - [30] D. S. Rokhsar, Phys. Rev. Lett. **79**, 2164 (1997).
 - [31] B. Jackson and C. F. Barenghi, Phys. Rev. A **74**, 043618 (2006).
 - [32] T. Giamarchi, C. Rüegg, and O. Tchernyshyov, Nature Physics **4**, 198 (2008).
 - [33] Magnon condensation experiments have included both cases out of equilibrium with magnon injection [6, 7], and also those using an applied magnetic field as an effective chemical potential (see e.g. [32] and Refs. therein); it is the former of these cases which is relevant here.